Hindawi Publishing Corporation
Advances in Materials Science and Engineering
Volume 2014, Article ID 390965, 9 pages
http://dx.doi.org/10.1155/2014/390965

Research Article

Optical Evaluation on Delamination Buckling of Composite Laminate with Impact Damage

J. T. Ruan,[1] F. Aymerich,[2] J. W. Tong,[3] and Z. Y. Wang[3]

[1] *School of Mechanical Engineering, Tianjin Key Laboratory of Advanced Mechatronics Equipment Technology, Tianjin Polytechnic University, Tianjin 300387, China*
[2] *Department of Mechanical Engineering, University of Cagliari, Cagliari 09123, Italy*
[3] *Department of Mechanics, Tianjin University, Tianjin 300072, China*

Correspondence should be addressed to J. W. Tong; tjw@tju.edu.cn

Received 16 October 2013; Revised 23 January 2014; Accepted 27 January 2014; Published 6 March 2014

Academic Editor: Jun Liu

The delamination buckling and growth behaviors of a cross-ply composite laminate with damage induced by low velocity impact are investigated optically using three-dimensional digital image correlation (3D-DIC) method. For the 3D deformation measurement, the 3D-DIC setup comprised of two CCD cameras was adopted. The rectangle specimen was impacted under the impact energy of 7.0 J using a drop-weight testing machine, and the impact damage was detected by means of X-ray nondestructive evaluation (NDE) technique. The 3D deformation field measured with the optical system clearly reveals that the delamination buckling characteristic of the specimen mainly appears local deformation mode under compression after impact test. Moreover, the behavior of delamination growth evaluated by the 3D-DIC optical method reasonably agrees with the NDE observed damage result after compression.

1. Introduction

Composite material is widely used in the structure components of aircraft and spacecraft because of its high specific strength and lightweight property. The increasing applications of composite material inevitably cause the risks from low velocity impact (LVI) damage by foreign object, such as a dropped tool or runway debris. The impact damage, mostly delamination, is especially dangerous for the composite structure because it is difficult to detect by visual inspection on the surface [1, 2]. Under in-plane compression, damaged composite laminate may generate delamination buckling and growth until the final failure of the structure [3]. In general, compression after impact (CAI) strength is considered as one of the most important issues in the design of composite structure. Therefore, it is necessary to better understand the deformation behavior of the damaged composite laminate under compression in order to effectively use it in structure engineering.

Numerous researchers focused their attentions on the CAI strength prediction and buckling analysis of composite laminates with embedded delaminations by the experimental method and numerical simulation [4–6]. In experimental studies, although the critical load is obtained from the load-displacement curve of the testing machine, the out-of-plane displacement of laminate is not experimentally measured under the delamination buckling test. In the literature [7], the deflections of composite plates containing multiple delaminations were measured at the center of both front and back surfaces using noncontact laser displacement meters. In another study [8], Gu and Chattopadhyay analogously used two linear variable displacement transducers (LVDTs) to measure the midpoint deflections of the delaminated layer and the sublaminate. These studies reveal that the out-of-plane deformation of composite laminated specimen plays an important role in the delamination buckling analysis. However, the displacement sensors can only measure the deflections of the given points.

The optical measurement techniques, which possess high precision, noncontact, and full-field advantages, have been widely used for measuring the displacement or strain fields of composite laminate. Shadow moiré was adopted to measure

the out-of-plane displacements of composite laminates with artificially manufactured delaminations under in-plane compressive loads [9–11]. Due to the substitution of holographic plates by CCD camera, electronic speckle pattern interferometry (ESPI) has significant advantages on the speed, easy use, and automatic measurement. The authors [12] measured the deformation of composite laminate with impact damage under compressive loads using carrier-ESPI method. However, ESPI is not suitable for measuring the deformation under the buckling test owing to the wavelength magnitude of measurement accuracy. To compare with the above optical methods, digital image correlation (DIC) technique is the most popular valuable tool in deformation measurement of object because of the simple specimen preparation and optical setup, especially the scalable spatial resolution that depended on the nature of the reference image [13, 14]. Lecomte-Grosbras et al. measured the interlaminar shear strain on the free edges of carbon/epoxy laminates using DIC technique [15]. Our group used the DIC method to measure the whole-field displacement around the hole in notched AS4/PEEK composite laminates and around the overlap end of laminated single-lap joints [16, 17]. The three-dimensional digital image correlation (3D-DIC) method, which combines DIC with stereo vision, is widely used to measure the profile and deformation on the surface of the object [18, 19]. The accurate measurement of full-field surface profile of a carbon fiber composite satellite antenna was investigated using 3D-DIC technique [20]. Melin and Schön used digital speckle photography (DSP) measurement system from the German company GOM mbH to determine the buckling shape and growth of impact-damaged carbon-fibre/epoxy composite laminates under fatigue load [21]. Rhead et al. employed a Limess VIC-3D HS DIC system to show the buckling modes of composite laminates subjected to in-plane free edge impact [22].

In this study, for evaluating the delamination buckling of damaged composite laminate, 3D measurements on the deformation process were experimentally investigated with the 3D-DIC method. The delamination buckling behavior of the impacted laminated specimen was analyzed by this optical method. For validating the performance of the 3D-DIC optical measurement method, the experimental results of 3D measurement were compared with the X-ray nondestructive evaluation (NDE) testing results after compression.

2. Experimental Study

2.1. Tested Specimen. The specimen used in this study was made from HS160/REM graphite/epoxy prepregs. The dimensions of specimen with the stacking sequence $[0_3/90_3]_S$ are $65 \times 87.5 \times 2.0\,\text{mm}^3$. In order to introduce the impact damage, a drop-weight testing machine was used for low velocity impact test. The impact energy applied on the specimen was 7.0 J by adjusting the drop height of impactor.

After the impact, impact damage (delaminations, matrix cracks, fibre fractures) was detected by means of NDE techniques. To obtain the highly detailed pictures of impact damage, penetrant-enhanced X-ray radiography was utilized to detect the impacted specimen after a radioopaque zinc iodide solution to infiltrate the damaged areas. This method can enhance the contrast of damage, but the internal damage not connected to the surface cannot be impregnated with the zinc solution and remains undetected. Therefore, the impacted specimen was ultrasonically inspected by C-scanning and analyzed with a specialized full-volume ultrasonic technique, which can reconstruct the internal damage of impacted sample and provide the information about the size and depth of selected delaminations. In order to eliminate the masking effect under scanning deeper damage, the specimen was examined from the two sides and the obtained information was recombined into a single image. The total delamination area measured by means of X-ray NDE technique was $432.1\,\text{mm}^2$ [23].

2.2. CAI Test. In CAI test, an antibuckling device was designed according to the recommendations of SACMA SRM 2R-94 [24], as shown in Figure 1. To prevent global buckling generated under compression, a pair of steel plates with a window of 29.4 mm × 67.5 mm was used in the antibuckling device. With this device, the local deformation will generate at the damaged zone. And it is prone to optically observe the delamination buckling as the compressive loading increases.

The impacted laminate was mounted into the antibuckling device with 0° direction parallel to the loading direction. The pair of steel plates were clamped in the slot of the base plate and supported at both sides by slide blocks and side supports with the knife edges. The gap between the knife edges could be adjusted to different thickness specimens through sliding the slide blocks. A servohydraulic testing machine with a maximum load capacity of 100 kN was employed. The load was applied on the specimen through a loading assembly. Four back-to-back strain gauges were attached on a high strength steel bar connected with the compression header to monitor the magnitude of load during compression.

2.3. Experimental Procedure. To measure the specimen deformation, the 3D-DIC experimental setup shown in Figure 2 was adopted. The setup was composed of two 8 bit gigabit Ethernet (GigE) CCD cameras (OK_AM1360, JoinHope Image Technology Ltd., Beijing, China) having a frame rate of 25 fps with the resolution of 1360 × 1024 pixels, which were used to simultaneously record the images of the impact back surface of specimen from two viewpoints.

To acquire the speckle pattern, the white paint was sprayed onto the specimen surface to generate random speckle-like field before testing. In addition, two white light sources were used to illuminate the composite specimen surface from two symmetrical directions to obtain high quality speckle images, as shown in Figure 2. It is noted that the two cameras have been rotated with the angle of 90 degrees to make the height of the specimen fill the entire width of the image. Therefore, the images taken from the two cameras have superior image resolution and the specimen in the captured images is displayed to put along the horizontal direction in this study.

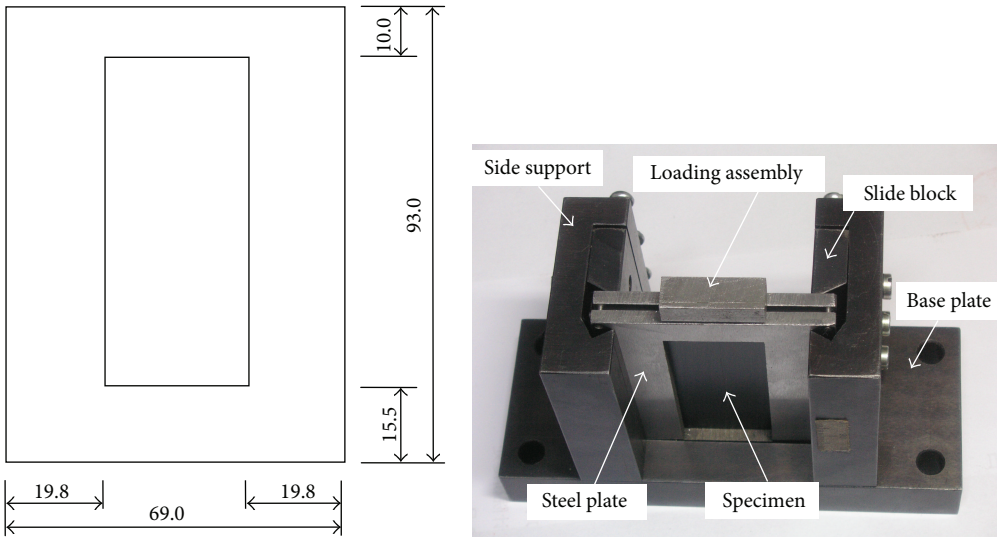

(a) Geometric dimensions of the steel plate (b) Photograph of the fixture

Figure 1: Compression testing device.

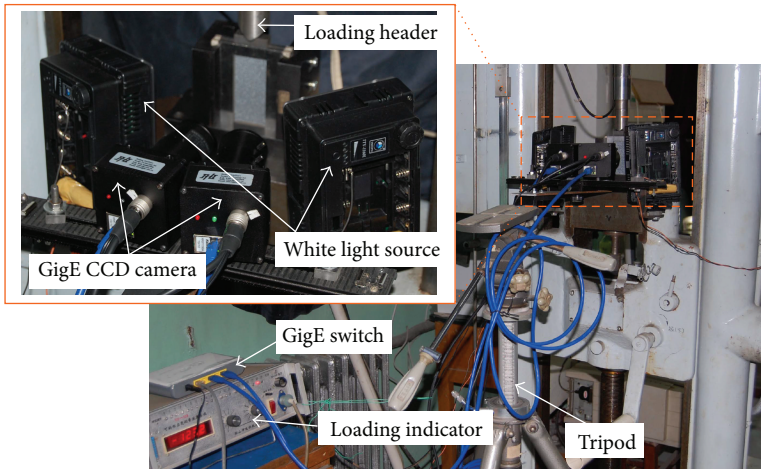

Figure 2: Experimental setup of 3D-DIC.

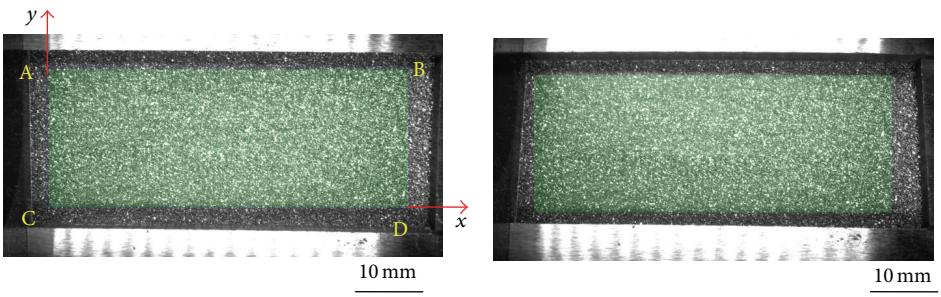

(a) Left image (b) Right image

Figure 3: A pair of images of specimen surface captured by the two cameras.

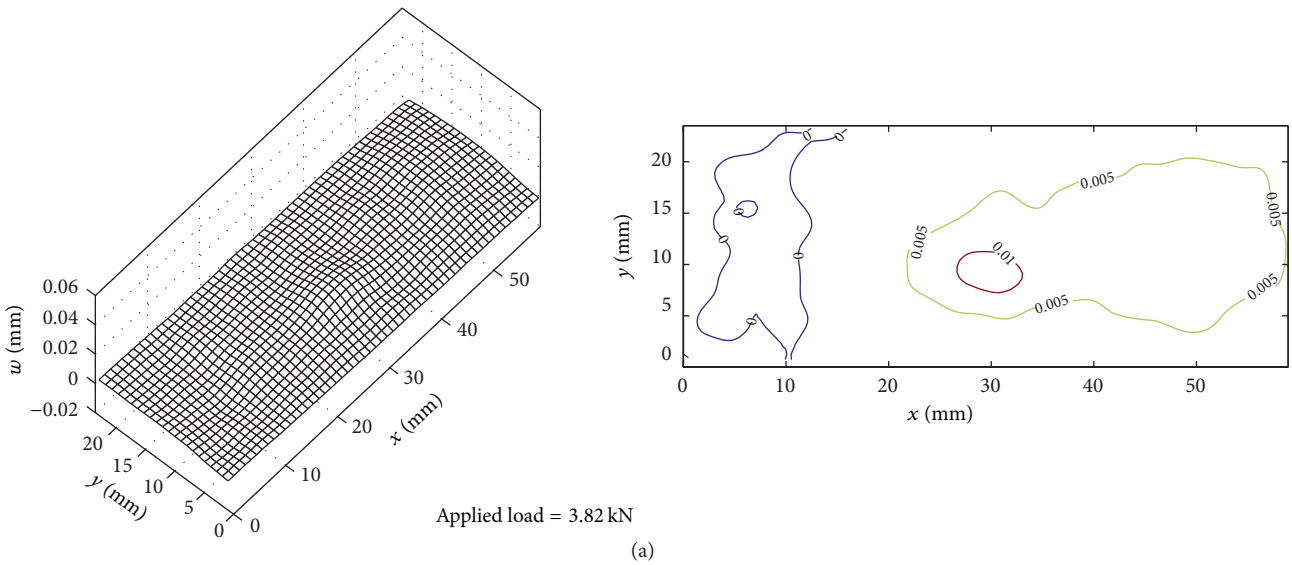

Applied load = 3.82 kN

(a)

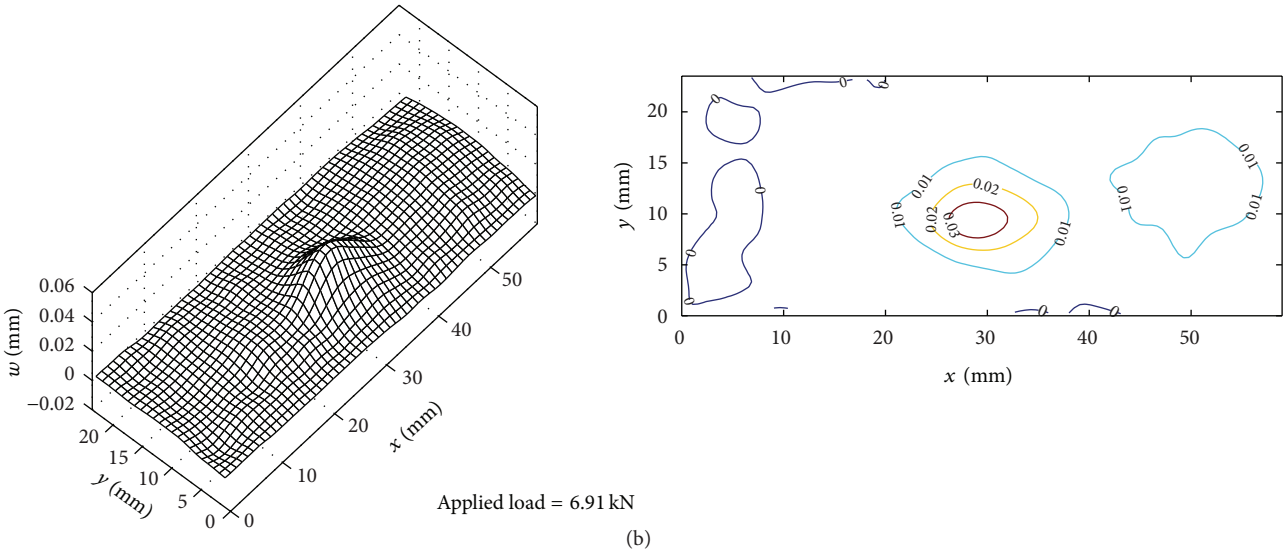

Applied load = 6.91 kN

(b)

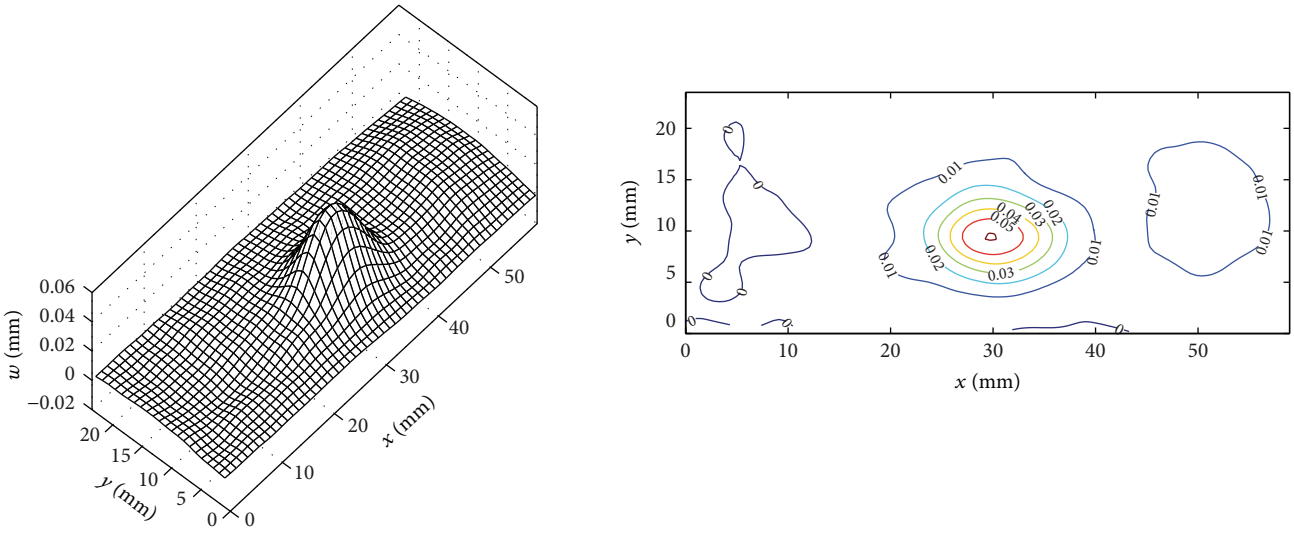

Applied load = 8.18 kN

(c)

Figure 4: Continued.

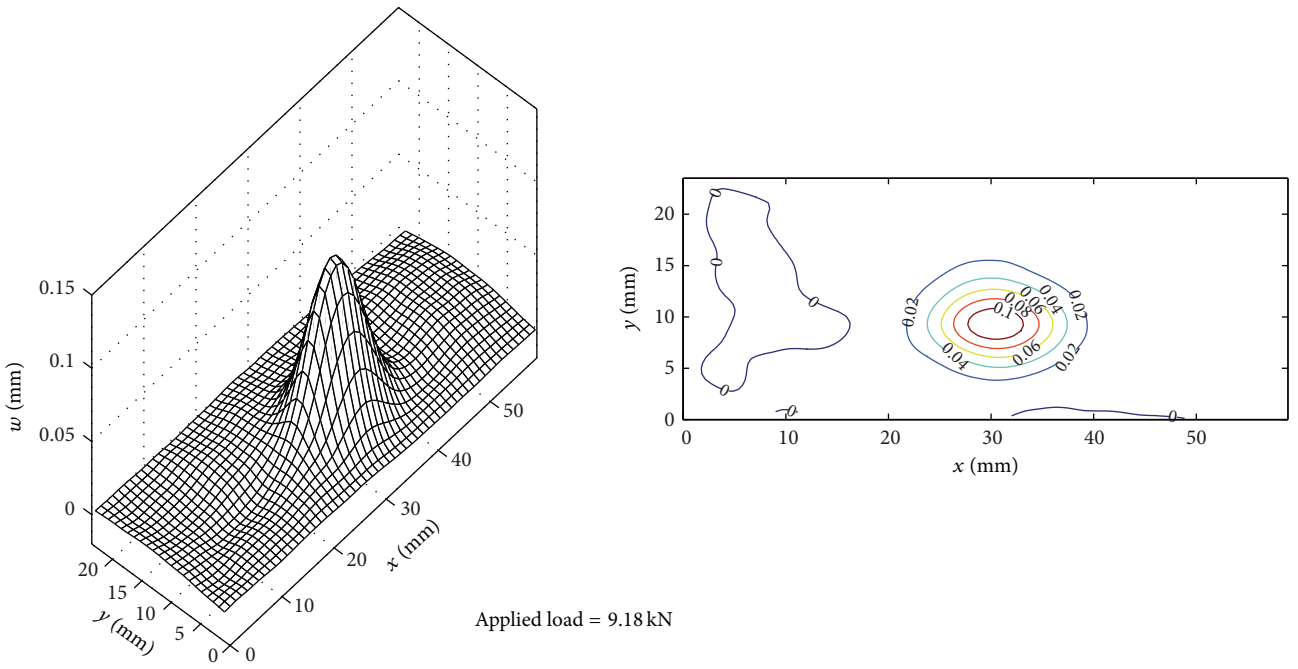

Figure 4: Measurement results of out-of-plane displacement under different load stages.

Before capturing the specimen images, the camera parameters were calibrated using a predetermined chessboard calibration pattern, which has 18 × 13 square grids with the side length of 3.0 mm. The calibration process consists of the following steps.

(i) Print the calibration pattern on an A4 paper with a laser printer and attach it to a flat glass plate.

(ii) Take a few pairs of images of the calibration pattern under different positions and orientations by moving or rotating the plane. In our experiment, twelve pairs of images were taken in total by both cameras during the calibration process.

(iii) Detect the coordinates of angular points in the images by the edge detection algorithm.

(iv) Estimate the intrinsic and extrinsic parameters using the flexible camera calibration technique, which is originally developed by Zhang [25].

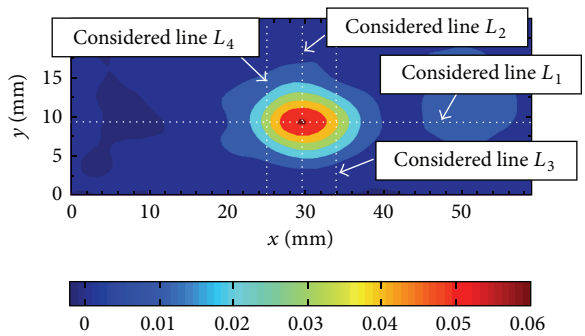

FIGURE 5: Locations of the considered lines.

After calibration, the pairs of images of specimen were simultaneously recorded under the states of different compressive loads. The out-of-plane displacement fields can be obtained with the 3D-DIC software developed in Visual C++ by ourselves.

3. Results and Discussion

Figure 3 shows a pair of images of the specimen surface captured by the left camera and right camera. During the correlation computing, the subset size was set to 41×41 pixels, and the grid steps in the x and y directions were both set to 10 pixels. The rectangle region of interest with the dimensions of 23 mm × 59 mm was measured for the calculation, as plotted with the dotted line in Figure 3. The corresponding magnification of the imaging system is 0.0525 mm/pixel. Therefore, the displacement accuracy can achieve about 1.05 μm because the displacement measurement precision in DIC is estimated as 0.02 pixels [13].

3.1. Delamination Buckling. To show the buckling behavior of specimen, the out-of-plane displacement fields evaluated with the optical measuring system are shown in Figure 4. Before the critical load (less than the level of 9 kN), the out-of-plane displacement is displayed on the same scale in both 3D and contour maps to observe the development of deformation.

Until the compressive load level reaches about 8.2 kN, the height of the bulged surface in 3D plot increases steadily. At the load of 9.18 kN, there is an evident increase of deformation, that is, a local buckling at the damaged area. The local buckling is even larger at the load of 11.36 kN because the delamination already propagates at this area and causes a considerable reduction of the specimen stiffness. It can be seen from the contour maps in Figure 4 that the shape of local deformation is oval. The long axis of the oval is along the horizontal direction, namely, the loading direction.

Figure 5 shows the locations of the considered lines for obtaining the plots of displacement distribution. The considered line L_1 locates at $y = 9.3$ mm along the x direction. The point with the maximum out-of-plane displacement is on these two lines. The x coordinate of vertical line L_2 is equal to 29.9 mm. The distances between the lines L_2, L_3 and L_2, L_4 are 4.1 mm and 4.4 mm, respectively.

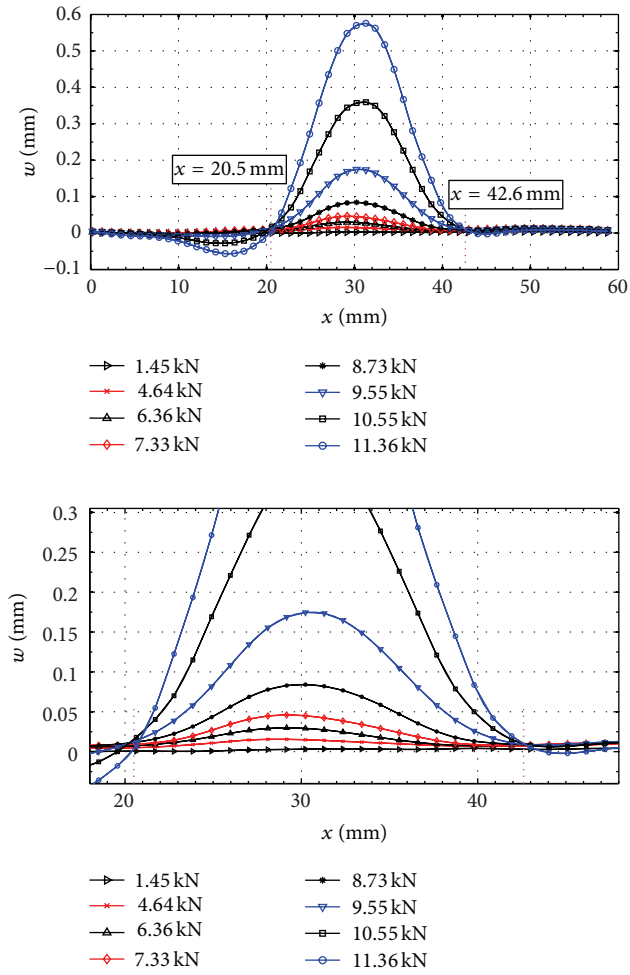

FIGURE 6: Out-of-plane displacement distribution of line L_1 with the change of compressive loads.

Figure 6 shows the out-of-plane displacement distribution of line L_1 along x direction for the specimen under different load levels. The location of L_1 is plotted in Figure 5. As it is seen in Figure 6, the local deformation is increased with the increment of loading. When the compressive loading reaches about 10 kN, the local deformation obviously appears at two locations and the deformation has opposite directions. It is caused by the fact that the off-axis load will be produced under the CAI tests for the thin laminated composite plate. Namely, the membrane-bending coupling effect causes a local convex deformation and a local concave deformation. The value of negative local deformation is smaller compared with the positive local deformation, which reaches approximately 0.06 mm at the final load of 11.36 kN.

To determine the boundary of local buckling and its extension, an enlarged view of the out-of-plane displacement distribution on line L_1 with the x coordinates ranging between 18 and 48 mm is simultaneously given. It can be seen in Figure 6 that the positive local deformation growth is along the positive x-axis and is infrequent along the negative x-axis. Therefore, the lower boundary of the deformation always maintains the location whose coordinate of x direction is

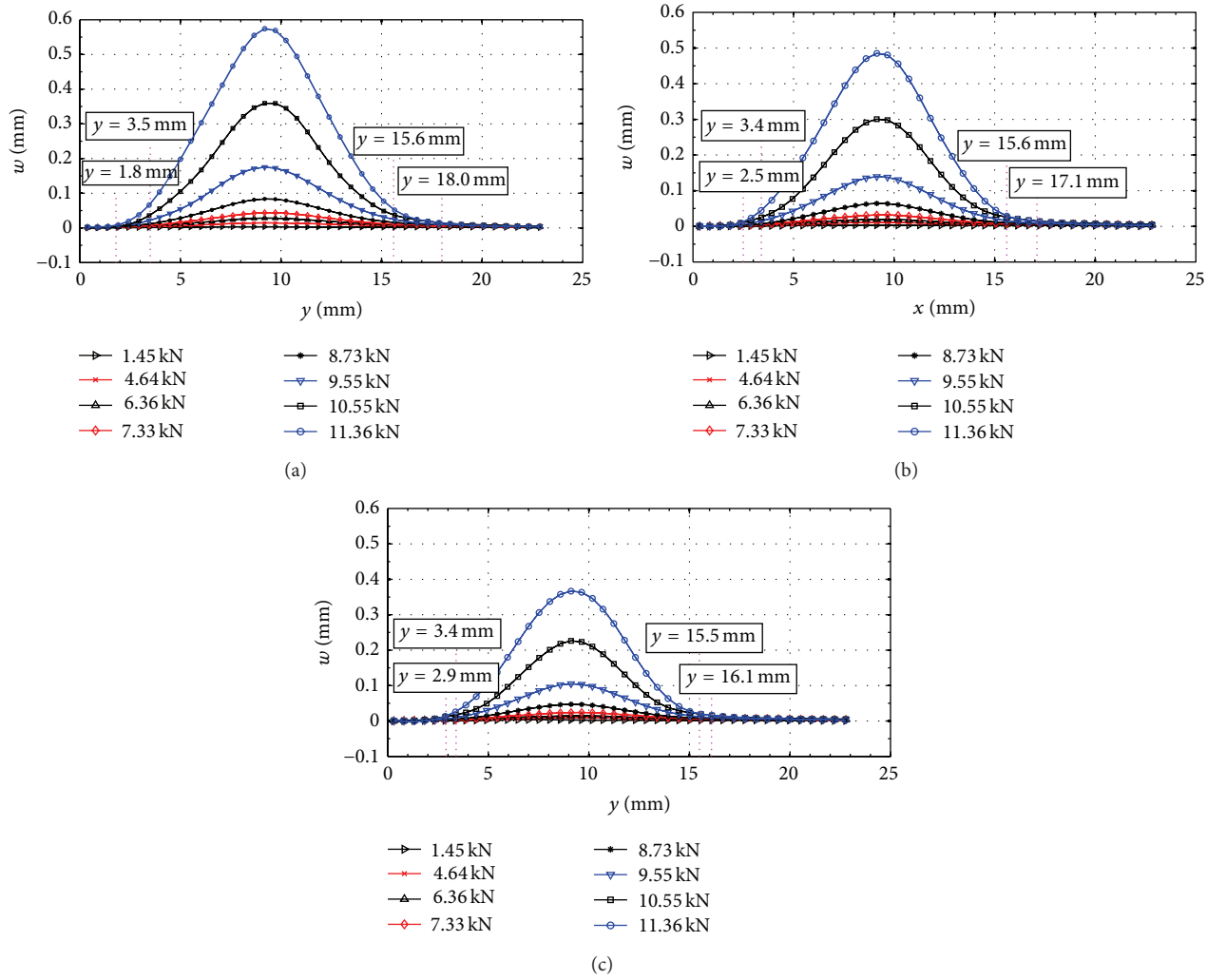

FIGURE 7: Displacement distribution on different vertical lines: (a) L_2, (b) L_3, and (c) L_4.

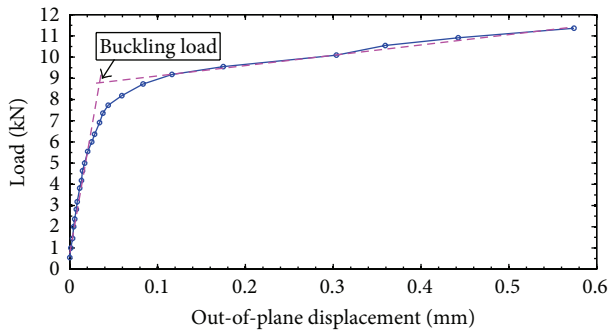

FIGURE 8: Relationship between the maximum out-of-plane displacement and compressive loads.

about 20.5 mm. For the upper boundary, it is approximately located at $x = 40$ mm when the compressive load is less than 8.73 kN. And the x coordinate extends to 42.6 mm when the ultimate load is equal to 11.36 kN. However, the negative local deformation does not extend along both positive and negative x directions. A conclusion can be drawn from the phenomenon that the delamination caused by low velocity impact only grows along the positive x direction and does not propagate along the negative x direction. The possible reason of this result is that the constraints of top and bottom ends of the specimen are different, as shown in Figure 1(b).

Figure 7 shows the out-of-plane displacement distributions of different vertical lines in the process of compression. Figure 7(a) shows the displacement distribution of L_2, whose location is plotted in Figure 5. According to Figure 7(a), the local deformation grows towards the positive and negative directions. When the compressive load is less than 8.73 kN, the y coordinates of lower and upper boundaries are 3.5 mm and 16.5 mm, respectively. With the increment of applied load, the two boundaries have extended to about 1.8 mm and 18.0 mm, respectively.

However, the growth of local deformation on both lines L_3 and L_4 is different from that of L_2, as shown in Figures 7(b) and 7(c). Figure 7(b) shows the displacement distribution of line L_3 with the expression of $x = 34.0$ mm. The upper boundary of local deformation extends from 15.6 mm to

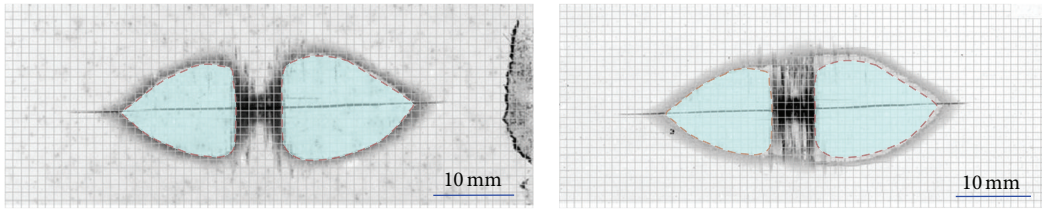

(a) (b)

Figure 9: X-radiographs of specimen before (a) and after (b) compression.

17.1 mm. Meanwhile, the lower boundary is located at y = 3.4 mm and changed into y = 2.5 mm. Therefore, the magnitude of local deformation growth of line L_3 is smaller than that of L_2. From the development of out-of-plane displacement on the line L_4 shown in Figure 7(c), it is observed that the local deformation growth is small and only propagates about 0.6 mm.

Figure 8 gives the relationship curve between the maximum out-of-plane displacement and applied compressive loads. It is observed that the values of out-of-plane are small and increase in an almost linear manner until the compressive load of about 6 kN. As the load becomes larger and exceeds the level of 8 kN, the change rate of out-of-plane displacement increases greatly. The buckling load is defined as the load value of the point where the straight line before buckling intersects the postbuckling linear part [26]. Therefore, the buckling load of the specimen is approximately 9 kN as seen in Figure 8.

3.2. Damage Assessment before and after Compression. To confirm the growth of delamination, the X-ray NDE technique was carried out to inspect the delamination damage. Figure 9 shows the X-radiographs of the specimen before and after compression. The delamination area before compression is highlighted by the dotted line and color region in these two X-radiographs. From this graph, the delamination growth evaluated with the 3D-DIC method is in a reasonable agreement with the measurement result by the X-ray NDE technique.

The delamination grows along the positive x direction, while it does not grow in the opposite direction. The magnitude of delamination growth is smaller than the result measured by the 3D-DIC optical method. The reason of this result is that the tip of delamination will close slightly when the specimen is unloaded. At the upper part of the specimen, the delamination propagates along the positive and negative y directions. The growth increment is similar to the experimental results. At the lower part, the delamination does not extend due to the fixed constraint. According to the X-radiograph of the specimen after compression in Figure 9(b), the delamination grows largely at the location of impact. However, this phenomenon cannot be shown in the experiment measurement.

It can be seen in Figure 9 that the tensile matrix crack does not extend before and after compression under the load level in this study. This impact damage is easily detected by the naked eyes. In contrast, the delamination is barely a visible impact damage (BVID) and grows in some degree under compression. Clearly, the 3D-DIC method can visually present the growth of delamination. This 3D optical measurement method can also be used to estimate the mechanical performance of laminate with impact-induced damage under CAI test.

4. Conclusions

The 3D measurement during the deformation process of graphite fiber/epoxy composite laminate with low velocity impact damage under compression was conducted using the 3D-DIC optical full-field measurement technique. The deformation behavior including delamination buckling and growth was evaluated with the optical measuring system.

Quantitative deformation profiles under different load stages were experimentally obtained. The specimen mainly presents the local deformation mode under CAI test with the designed testing device. Moreover, the local deformation only grows towards the positive x direction, whereas the growth of the local deformation generates along the two directions of the y-axis. The optical measurement results are verified by comparing with the NDE test result of delamination damage after compression.

The experimental results confirm the effectiveness of the optical measuring method in gaining a better understanding of the deformation characteristics of the specimen. Therefore, the 3D-DIC method is a powerful and useful tool for quantitatively evaluating the delamination buckling behavior of the composite laminate during compression after impact.

Conflict of Interests

The authors declare that there is no conflict of interests regarding the publication of this paper.

Acknowledgments

The authors are grateful to the National Natural Science Foundation of China (Grant number 11102134), the Colleges and Universities Science and Technology Development Foundation of Tianjin (Grant number 20130903), and the European Union Foundation (Grant number FP7-PEOPLE-ITN 238325) for financial support.

References

[1] S. R. Finn, Y. He, and G. S. Springer, "Delaminations in composite plates under transverse impact loads-experimental results," *Composite Structures*, vol. 23, no. 3, pp. 191–204, 1993.

[2] M. O. W. Richardson and M. J. Wisheart, "Review of low-velocity impact properties of composite materials," *Composites A*, vol. 27, no. 12, pp. 1123–1133, 1996.

[3] L. E. Asp, S. Nilsson, and S. Singh, "An experimental investigation of the influence of delamination growth on the residual strength of impacted laminates," *Composites A*, vol. 32, no. 9, pp. 1229–1235, 2001.

[4] D. Ghelli and G. Minak, "Low velocity impact and compression after impact tests on thin carbon/epoxy laminates," *Composites B*, vol. 42, no. 7, pp. 2067–2079, 2011.

[5] Z. Aslan and M. Şahin, "Buckling behavior and compressive failure of composite laminates containing multiple large delaminations," *Composite Structures*, vol. 89, no. 3, pp. 382–390, 2009.

[6] S. F. Hwang and G. H. Liu, "Buckling behavior of composite laminates with multiple delaminations under uniaxial compression," *Composite Structures*, vol. 53, no. 2, pp. 235–243, 2001.

[7] H. Suemasu, T. Irie, and T. Ishikawa, "Buckling and post-buckling behavior if composite plates containing multiple delaminations," *Journal of Composite Materials*, vol. 43, no. 2, pp. 191–202, 2009.

[8] H. Gu and A. Chattopadhyay, "An experimental investigation of delamination buckling and postbuckling of composite laminates," *Composites Science and Technology*, vol. 59, no. 6, pp. 903–910, 1999.

[9] S. S. Suh, N. L. Han, J. M. Yang, and H. T. Hahn, "Compression behavior of stitched stiffened panel with a clearly visible stiffener impact damage," *Composite Structures*, vol. 62, no. 2, pp. 213–221, 2003.

[10] D. S. Cairns, P. J. Minguet, and M. G. Abdallah, "Theoretical and experimental response of composite laminates with delaminations loaded in compression," *Composite Structures*, vol. 27, no. 4, pp. 431–437, 1994.

[11] M. Tuttle, P. Singhatanadgid, and G. Hinds, "Buckling of composite panels subjected to biaxial loading," *Experimental Mechanics*, vol. 39, no. 3, pp. 191–201, 1999.

[12] J. Ruan, S. Wang, J. Tong, M. Shen, F. Aymerich, and P. Priolo, "Deformation measurement of composite laminate with impact damage under compressive loads," *Polymers and Polymer Composites*, vol. 20, no. 1-2, pp. 177–182, 2012.

[13] B. Pan, K. M. Qian, H. M. Xie, and A. Asundi, "Two-dimensional digital image correlation for in-plane displacement and strain measurement: a review," *Measurement Science and Technology*, vol. 20, no. 6, Article ID 062001, 2009.

[14] B. Pan, "Recent progress in digital image correlation," *Experimental Mechanics*, vol. 51, no. 7, pp. 1223–1235, 2011.

[15] P. Lecomte-Grosbras, B. Paluch, M. Brieu, G. D. Saxcé, and L. Sabatier, "Interlaminar shear strain measurement on angle-ply laminate free edge using digital image correlation," *Composites A*, vol. 40, no. 12, pp. 1911–1920, 2009.

[16] Z. Y. Wang, H. Q. Li, J. W. Tong, M. Shen, F. Aymerich, and P. Priolo, "Dual magnification digital image correlation based strain measurement in CFRP Laminates with open hole," *Composites Science and Technology*, vol. 68, no. 9, pp. 1975–1980, 2008.

[17] Z. Y. Wang, L. Wang, W. Guo, H. Deng, J. W. Tong, and F. Aymerich, "An investigation on strain/stress distribution around the overlap end of laminated composite single-lap joints," *Composite Structures*, vol. 89, no. 4, pp. 589–595, 2009.

[18] P. F. Luo, Y. J. Chao, M. A. Sutton, and W. H. Peters III, "Accurate measurement of three-dimensional deformations in deformable and rigid bodies using computer vision," *Experimental Mechanics*, vol. 33, no. 2, pp. 123–132, 1993.

[19] M. A. Sutton, J. J. Orteu, and H. W. Schreier, *Image Correlation for Shape and Deformation Measurements Basic Concepts, Theory and Applications*, Springer, New York, NY, USA, 2009.

[20] B. Pan, H. Xie, L. Yang, and Z. Wang, "Accurate measurement of satellite antenna surface using 3D digital image correlation technique," *Strain*, vol. 45, no. 2, pp. 194–200, 2009.

[21] L. G. Melin and J. Schön, "Buckling behaviour and delamination growth in impacted composite specimens under fatigue load: an experimental study," *Composites Science and Technology*, vol. 61, no. 13, pp. 1841–1852, 2001.

[22] A. T. Rhead, D. Marchant, and R. Butler, "Compressive strength of composite laminates following free edge impact," *Composites A*, vol. 41, no. 9, pp. 1056–1065, 2010.

[23] F. Aymerich and P. Priolo, "Characterization of fracture modes in stitched and unstitched cross-ply laminates subjected to low-velocity impact and compression after impact loading," *International Journal of Impact Engineering*, vol. 35, no. 7, pp. 591–608, 2008.

[24] "SACMA SRM 2R-94, Recommended test method for compression after impact properties of oriented fiber-resin composites," Arlington, VA: Suppliers of Advanced Composite Materials Association.

[25] Z. Y. Zhang, "A flexible new technique for camera calibration," *IEEE Transactions on Pattern Analysis and Machine Intelligence*, vol. 22, no. 11, pp. 1330–1334, 2000.

[26] M. R. Parlapalli, K. C. Soh, D. W. Shu, and G. Ma, "Experimental investigation of delamination buckling of stitched composite laminates," *Composites A*, vol. 38, no. 9, pp. 2024–2033, 2007.